Supplementary Material

1. Evaluation of simulated carbonate chemistry and related ocean dynamics

Here we briefly evaluate the UVic model's ability to simulate the ocean chemistry and physical dynamics that are relevant for this study. We first evaluate the model's capacity to simulate present-day ocean total alkalinity and oceanic dissolved inorganic carbon by making comparisons to GLODAP observational data (Key *et al* 2004). However, since the observations are very limited in the regions where we implement our AOA experiments (figure S1, figure S2), validating the model with only this data is difficult. In the portion of the Great Barrier Reef region that is available for comparison we find that the difference in surface alkalinity and dissolved inorganic carbon between the model and the observations are both around 11 mol/m^3. For regions where no AOA is simulated, the surface total alkalinity and dissolved inorganic carbon are higher than the GLODAP data in the Southern Ocean and the North Pacific. Underestimations exist in the east and west equatorial regions for both total alkalinity and dissolved inorganic carbon.

Since GLODAP data was limited in the areas where we simulated AOA we next compare the simulated oceanic pCO$_2$ global distribution with Surface Ocean CO$_2$ Atlas average data from year 1998 through 2011 (SOCAT) (Bakker *et al* 2014, Landschützer *et al* 2014), since this variable also provides some information on how well the model simulates ocean carbonate chemistry. Specifically, we compare (figure S3) with a global annual climatology (1°×1°) of sea surface pCO$_2$ derived from SOCAT data by (Landschützer *et al* 2014) using a neural network-based method. Note that the number of observations in the SOCAT database is also limited in our study regions (Bakker *et al* (2014), their figure 2 and figure 8). The comparisons of surface ocean pCO$_2$ between the UVic model and the climatological data generally show that the models performance is reasonable. On a regional scale, we find that UVic overestimates surface seawater pCO$_2$ by 27.34±2.5 μatm (GB),

1   17.83 ±5.4 μatm (CS) and 33.28±11.0 μatm (SC) in the GB, CS and SC regions,

2   respectively. Larger disagreement is found at high latitudes and in the equatorial East Pacific

3   with the model overestimating surface pCO_2 by up to 100 μatm at specific grid points. This

4   could either be due to UVic's relatively weak simulation of equatorial upwelling or the lack

5   of a dynamic atmosphere. This disagreement could be due to residuals between data and

6   the neural network-based climatology itself in those areas (figure 2 of Landschützer *et al*

7   (2014)). We exemplarily refer to MPI-ESM for checking how well our model does versus

8   such more complex Earth system models. The UVic model did not do any worse than the

9   broadly used MPI-ECM (Ilyina *et al* (2013), their figure 2 and figure 3), in which HAMOCC

10   model's surface pCO_2 has a variance of 40 μatm spatially and a general overestimation

11   globally with 50~150 umol/kg (equivalent to 0.050 ~ 0.150 mol/m3).

12   Sea Surface Temperature (SST) is commonly used as an important indicator to evaluate

13   modelled ocean circulation and thermodynamics (Wang *et al* 2014). SST simulated by UVic

14   is validated against World Ocean Atlas (WOA) 2013 climatology (Locarnini *et al* 2013). This

15   simulated SST distribution agrees well with the WOA (figure S4) except for a warm bias in

16   the subpolar North Pacific, eastern Equatorial Pacific and smaller regions in the Southern

17   Ocean. Simulated SST is also too low in Atlantic Ocean, especially at higher latitudes. In

18   some specific regions such as Northwest Pacific, the model-data difference can be as large as

19   6°C at some grid points. We find the magnitude of local/regional differences to be similar to

20   what is observed in CMIP5 models. Such biases are common in all global models as shown in

21   an analysis by Wang *et al* (2014), who found that CMIP5 models on average appear to have a

22   stronger and more widespread warm bias in the Southern Ocean, a stronger cold bias in the

23   subtropical ocean and North Pacific/Atlantic Oceans. In contrast to most CMIP5 models that

24   have a moderate cold bias in the North Pacific, UVic displays a large warm bias in this

25   region. One reason for this difference is the lack of a dynamic atmosphere in the UVic model.

26   Importantly, however, regions to which we apply AOA in our study are not characterized by

27   particularly large model-data SST misfits. For the regions where AOA is implemented,

28   UVic's RMS model-data SST misfit is less than 0.8 °C.

We also estimated the potential impacts of model biases in simulated carbonate chemistry on our AOA model results. A rigorous bias-correction process would require observational DIC and TA data from our AOA regions, which is unfortunately not available based on published data sets such as GLODAP. However, in our AOA regions, observational pCO2 and SST are accessible. Variations in the oceanic buffer factor depend mainly on changes in oceanic pCO2 and the ratio of DIC to TA. A bias in pCO2 can thus induce a bias in the ocean buffer factor and the sea surface aragonite Ω change per unit alkalinity addition. To estimate this possible bias, we first use model generated values of pCO_2, TA, SST and sea surface salinity (SSS) to calculate a model-based sea surface aragonite Ω through CO2sys (Lewis and Wallace 1998, van Heuven *et al* 2009). Assuming TA and SSS are unbiased, we use observational pCO_2 and SST data to estimate a bias-corrected sea surface aragonite Ω through CO2sys, too (Table S1). This estimated bias-corrected sea surface aragonite Ω from GB and SC is 6% and 5% higher than the model-based aragonite Ω. Without (with) bias corrected values of pCO_2 and SST, the aragonite Ω increments per unit alkalinity addition (computed from the model results of the first year of AOA, see table S1) amount to 4.15 (4.29) m^3/mol in GB, 3.37 (3.11) m^3/mol in CS and 3.39 (3.526) m^3/mol in SC. The estimated biases in omega translate into an uncertainty of required lime additions of roughly 3% more (GB), 7% less (CS) and 4% more (SC).

1

2
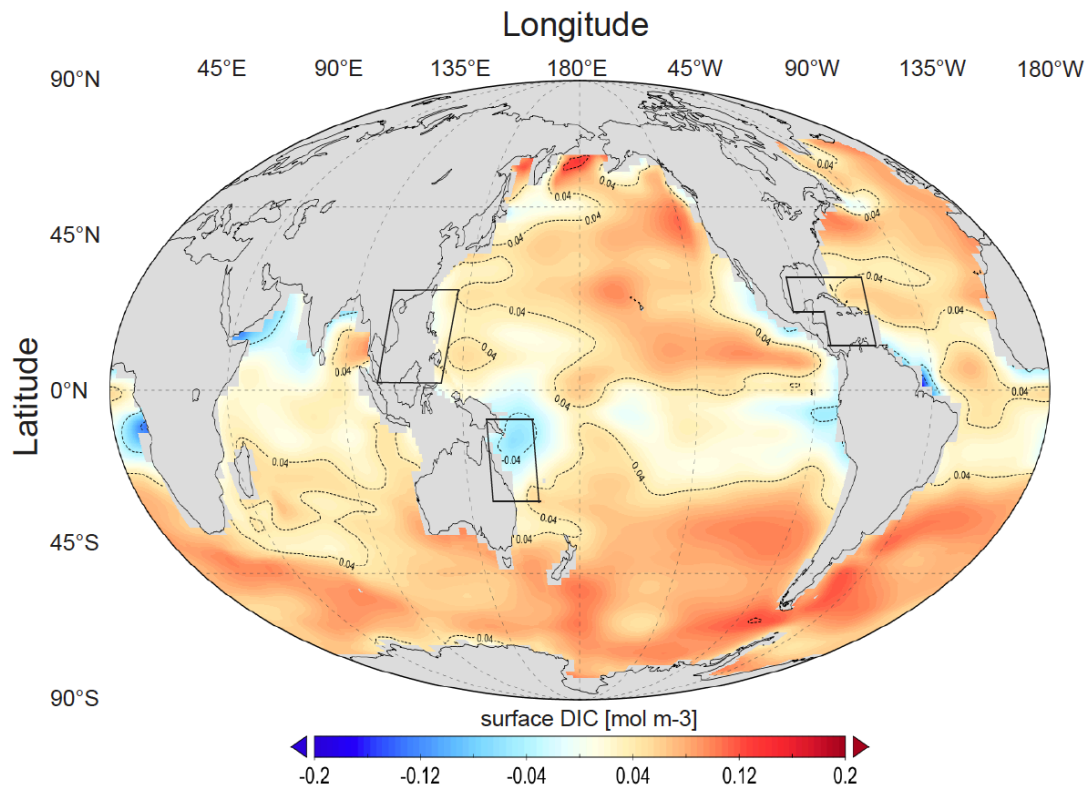

surface total alkalinity [mol m-3]

3
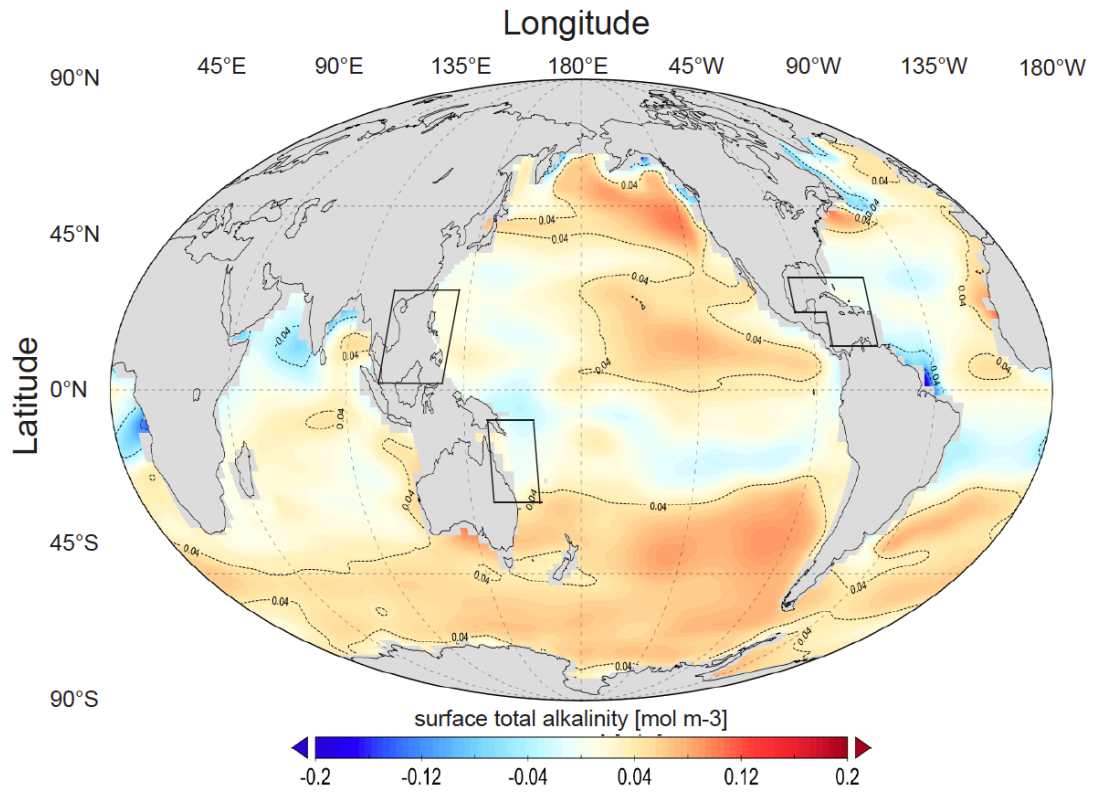
Figure S1. The sea surface total alkalinity difference between the UVic model (year 2020)

and GLODAP v1 data (Key *et al* 2004). UVic's data is regrided to fit GLODAP's 1°×1°

spatial resolution. GLODAP vertical total alkalinity data was averaged over the first 50

meters to be comparable with the UVic surface grid box height of 50m.

Figure S2. The sea surface dissolved inorganic carbon (DIC) difference between the UVic model (year 2020) and GLODAP v1 data (Key *et al* 2004). UVic's data is regrided to fit GLODAP's 1° ×1° spatial resolution. GLODAP vertical DIC data was averaged over the first 50 meters to be comparable with the UVic surface grid box height of 50m.
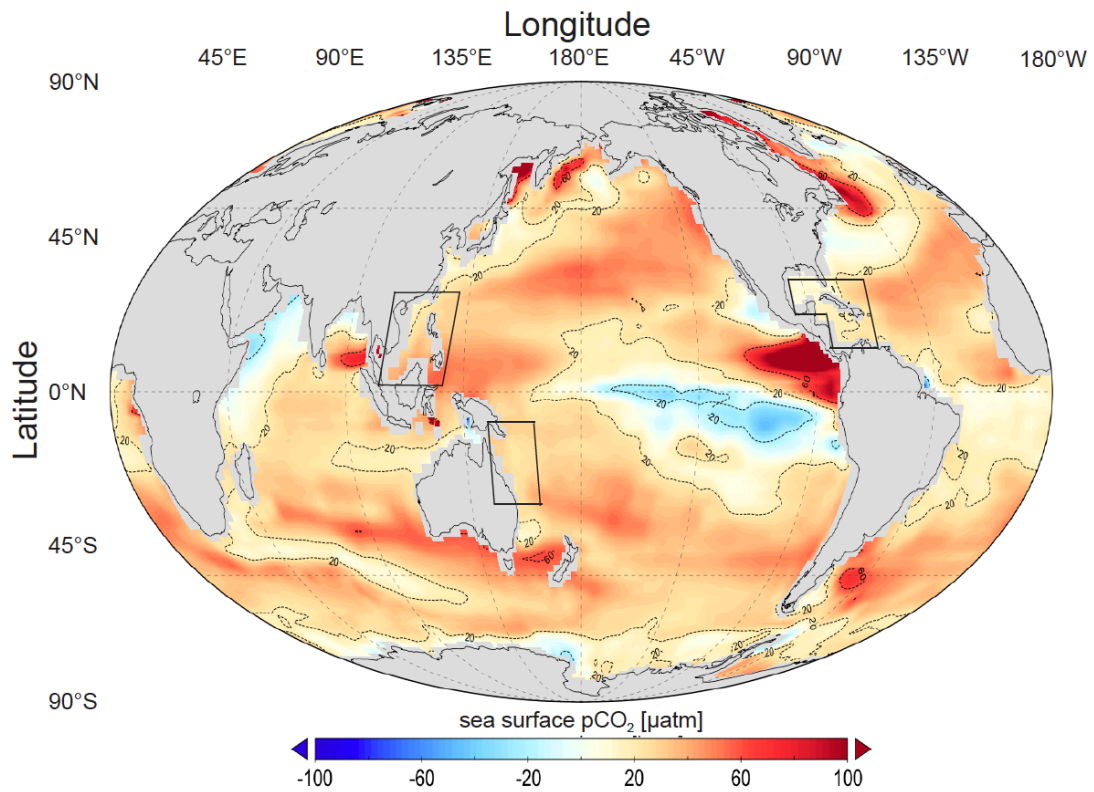
Figure S3. Global distribution for sea surface pCO$_2$ difference between UVic model (year 2020) and a SOCAT data based climatology (Landschützer *et al* 2014). UVic's data is regrided to fit SOCAT's 1° ×1° spatial resolution. SOCAT vertical pCO$_2$ data was averaged over the first 50 meters to be comparable with the UVic surface grid box height of 50m.

1
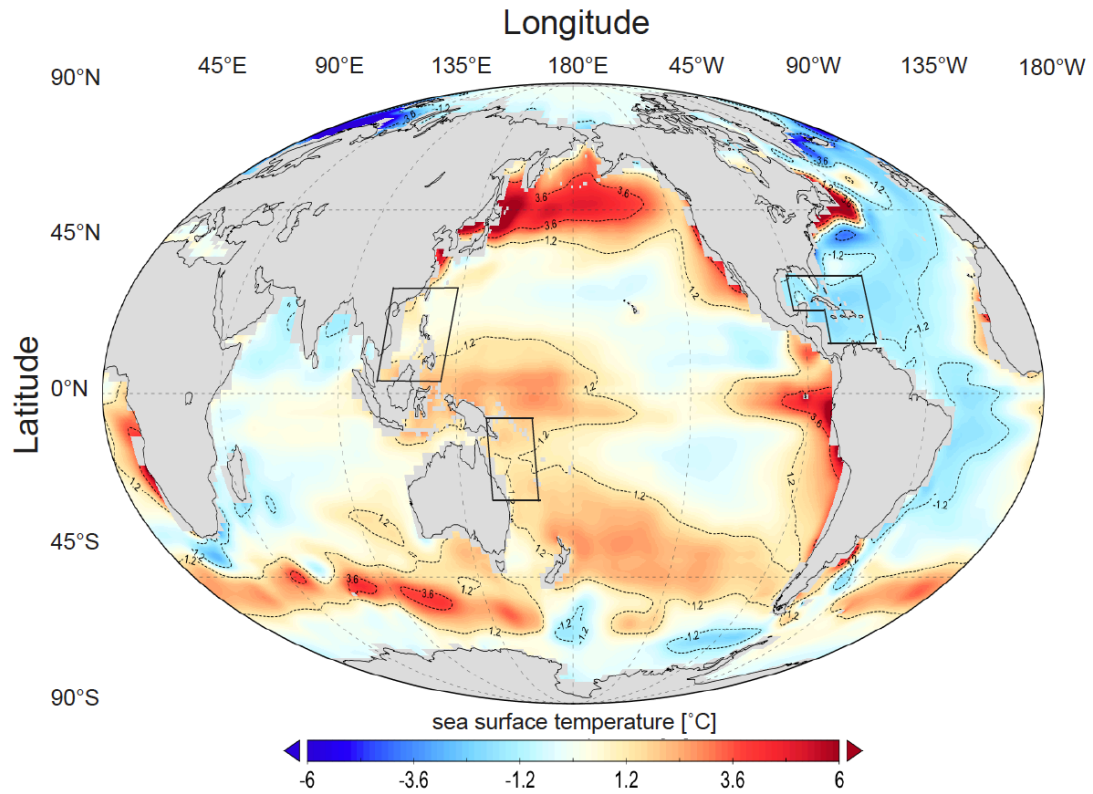
Figure S4. Global distribution for sea surface temperature (SST) difference between UVic

model (year 2020) and World Ocean Altas (WOA) 2013 climatology data (Locarnini *et al*

2013). UVic's data is regrided to fit WOA's 1°×1°spatial resolution. WOA vertical

temperature data was averaged over the first 50 meters to be comparable with the UVic

surface grid box height of 50m.

7

1

Table S1. Carbonate chemistry variables for model year 2020 (and 2021, the first year of AOA). Variables are regionally averaged from Great Barrier Reef (GB), Caribbean Sea (CS) and South China Sea (SC).   Inputs from model runs and corresponded output are gathered in "non-bias-correction" rows, while the same for observations are gathered in "bias-correction" rows (non-bias-corrected variables in those rows are left blank).

	Sea surface pCO_2 [µatm]	Sea surface TA [mol/m^3]	SST [°C]	SSS [‰]	ΔTA [mol/m^3]	Ω_{2020}	Ω_{2021}	$\Delta\Omega/\Delta$TA
GB (non-bias-correction)	179.3	2.643	27.75	34.84	0.20	7.065	7.894	4.15
GB (bias correction)	151.9		26.62			7.401	8.259	4.29
CS (non-bias-correction)	251.0	2.563	25.30	35.31	0.127	3.89	4.318	3.37
CS (bias-correction)	251.0		26.67			3.884	4.279	3.11
SC (non-bias-correction)	272.6	2.386	28.67	33.79	0.095	4.984	5.306	3.39
SC (bias-correction)	238.5		27.47			5.241	5.576	3.53

Abbreviation notes: TA (total alkalinity); SST (sea surface temperature); SSS (sea surface salinity); ΔTA (regional mean sea surface alkalinity change due to AOA from year 2020 to year 2021); Ω_{2020} (regional mean sea surface aragonite Ω in year 2020); Ω_{2021} (regional mean sea surface aragonite Ω in year 2021); $\Delta\Omega/\Delta$TA (sea surface aragonite Ω change per unit total alkalinity change)

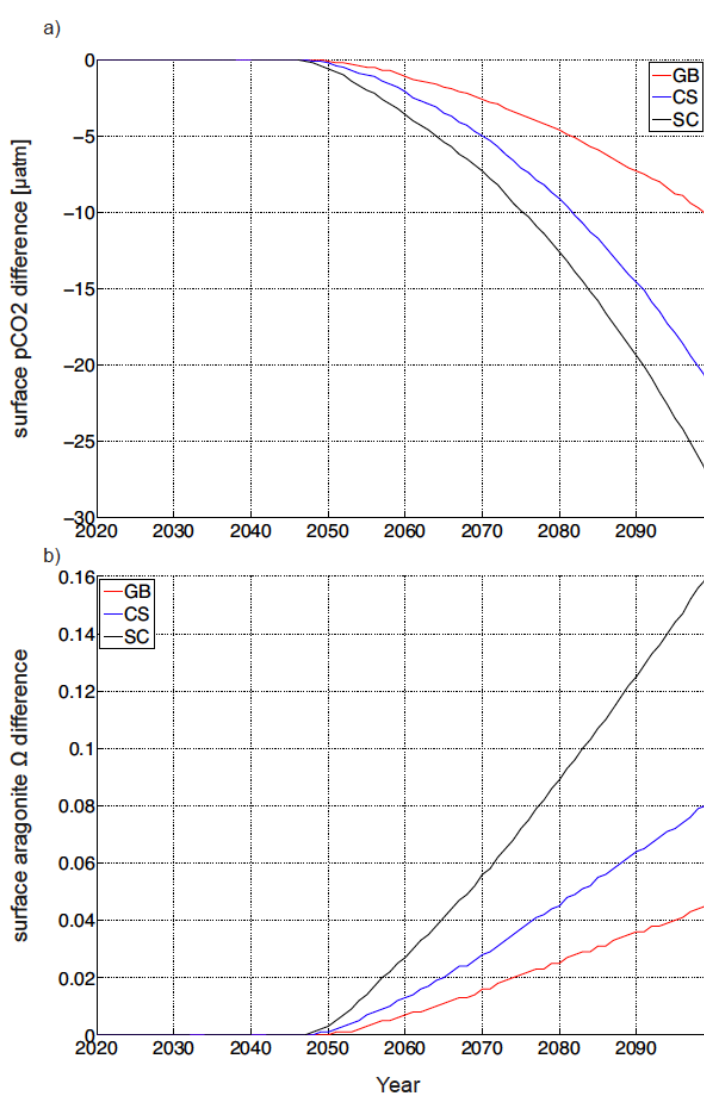2
3

1

2. Artificial Ocean Alkalinization (AOA) impacts on global mean surface aragonite Ω and pCO_2 levels

We calculate the global mean surface aragonite Ω and pCO_2 levels to investigate if the optimal AOA scheme will significantly perturb the global carbon cycle as illustrated for global mean surface aragonite Ω and pCO_2 in figure S5.


Figure S5. Time series of the simulated global annual mean surface pCO_2 level (a) and surface aragonite Ω level difference (b) between the optimal runs from Ensemble C and the control run.

1

3. AOA perturbation to the ocean surface dissolved inorganic carbon system

Adding calcium hydroxide would perturb the local marine dissolved inorganic carbon (DIC) system. Considering three different theoretical scenarios (invasion of anthropogenic CO_2, AOA-closed system and AOA open system), we calculated the changes of CO_2 (aq), carbonate and bicarbonate concentrations using the Matlab®-version of CO2SYS (Lewis and Wallace 1998, van Heuven *et al* 2009) and present results in Bjerrum plots (Wolf-Gladrow *et al* 2007) as a part of the perturbation protocol. Here CO_2 (aq) represents the sum of carbonate acid (H_2CO_3) and soluble CO_2 (Pilson 2013). Considering ocean acidification without AOA, CO_2 (aq) and bicarbonate ions will increase while carbonate ions decrease, which then causes the aragonite saturation state to decline (figure S6(a)) and the pH to become lower. If we consider a closed system (no air-sea gas exchange) of a water sample under continuous AOA, CO_2 (aq) and bicarbonate will both decline, while carbonate ions increase (figure S6(b)) along with pH. This demonstrates the chemistry behind using AOA to prevent ocean acidification and enhance the local aragonite saturation state. This situation can also serve as an analogue for either an abrupt AOA addition for a short time period or a very large AOA scheme where CO_2 invasion can be neglected. However, local AOA, like in our study, has a very limited impact on the pCO_2 of the well-mixed atmosphere. Hence, finally, we consider the case of an open system, where AOA is optimized to keep seawater pCO_2 approximating to a fixed value of 500 μatm but still allow for CO_2 invasion. For this case we find that there is a tendency for both carbonate and bicarbonate to increase together with a slight increase of pH (figure S6(c), S6(d)).

1
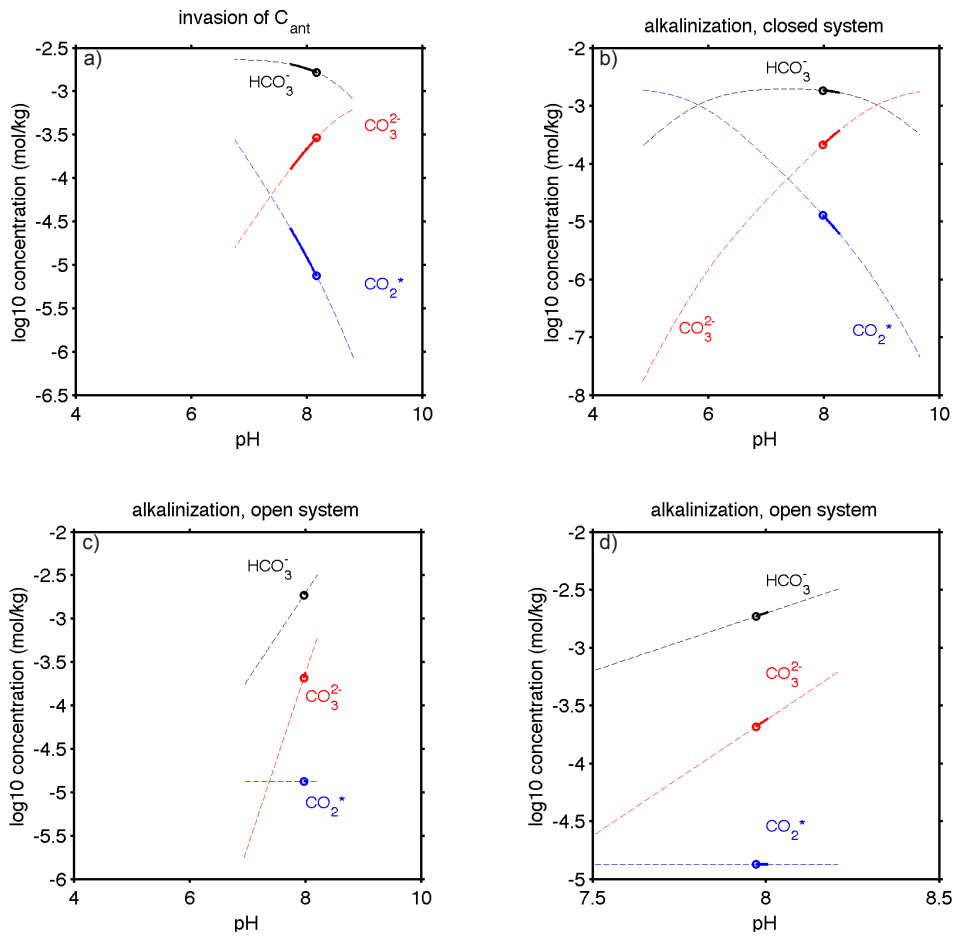
Figure S6. The marine dissolved inorganic carbon system under ocean acidification and

AOA. (a) is for a case without alkalinization but with the invasion of anthropogenic CO_2. (b)

is for a hypothetical closed system case (no air-sea gas exchange) with alkalinization of a

water sample initially equilibrated with an atmospheric pCO_2 of 500 μatm. (c) is for an open

system case optimized to fix the oceanic pCO_2 to 500 μatm. (d) is the same as (c) but with a

zoomed-in scale to show more detail.

8

1

4. Calcium change due Artificial Ocean Alkalinisation (AOA)

3   In our AOA experiments we change alkalinity assuming the addition of $Ca(OH)_2$, which

has an Alkalinity: Calcium (Ca) stoichiometric ratio of 2. We estimate the change in Ca

concentration over time by computing the alkalinity difference (AOA-control) and dividing

by 2. Results for Ensemble C's optimal simulations are shown in figure S7 as an example.

The maximum calcium elevation happens in year 2099, where the GB (Great Barrier Reef)

reaches a value of 0.16 mmol/kg, the CS (Caribbean Sea) of 0.26 mmol/kg and the SC (South

China Sea) of 0.34 mmol/kg. These increases are small compared to the background Ca

concentration of 10.27 mmol/kg (Pilson 2013).
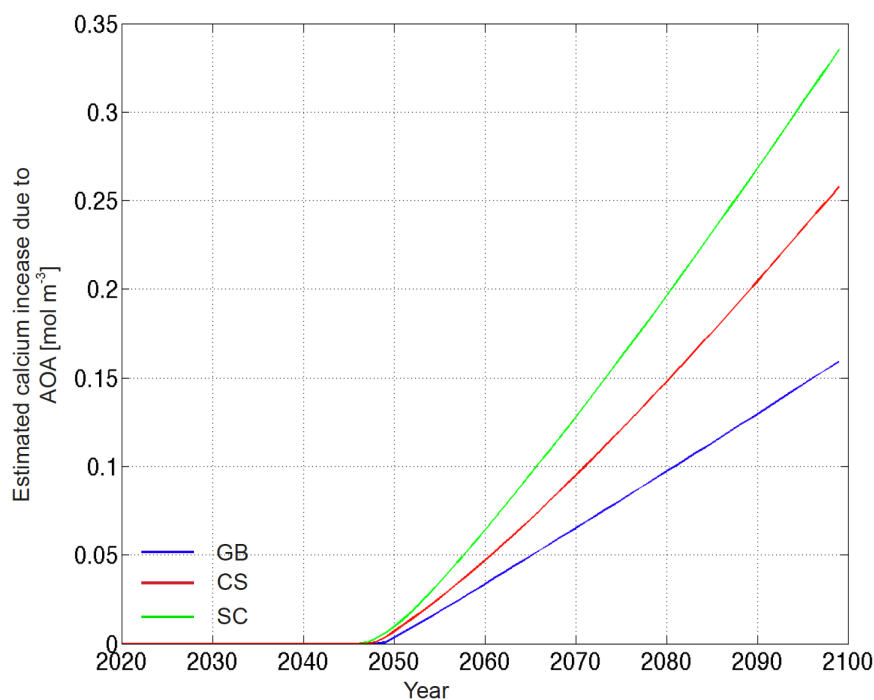
Figure S7. Estimated annual mean calcium increase in the respective regions for the

Ensemble C's optimal simulations. SC represents the "South China Sea", CS the "Caribbean

Sea" and "GB" the Great Barrier Reef region.

1   **5.   AOA induced sub-surface alkalinity change.**

2   Changes in alkalinity in sub-surface waters as a result of surface AOA in our regions of

3   interests are investigated here (figure S8, figure S9). We first look into the zonally averaged

4   vertical alkalinity change between the optimal runs and control run in year 2099 in the AOA

5   regions (figure S8). The next figure (figure S9) shows the total alkalinity change on

6   horizontally averaged chemistry within AOA implemented regions of the optimal runs. The

7   longitude dimension only covers the AOA implemented regions for both figures.
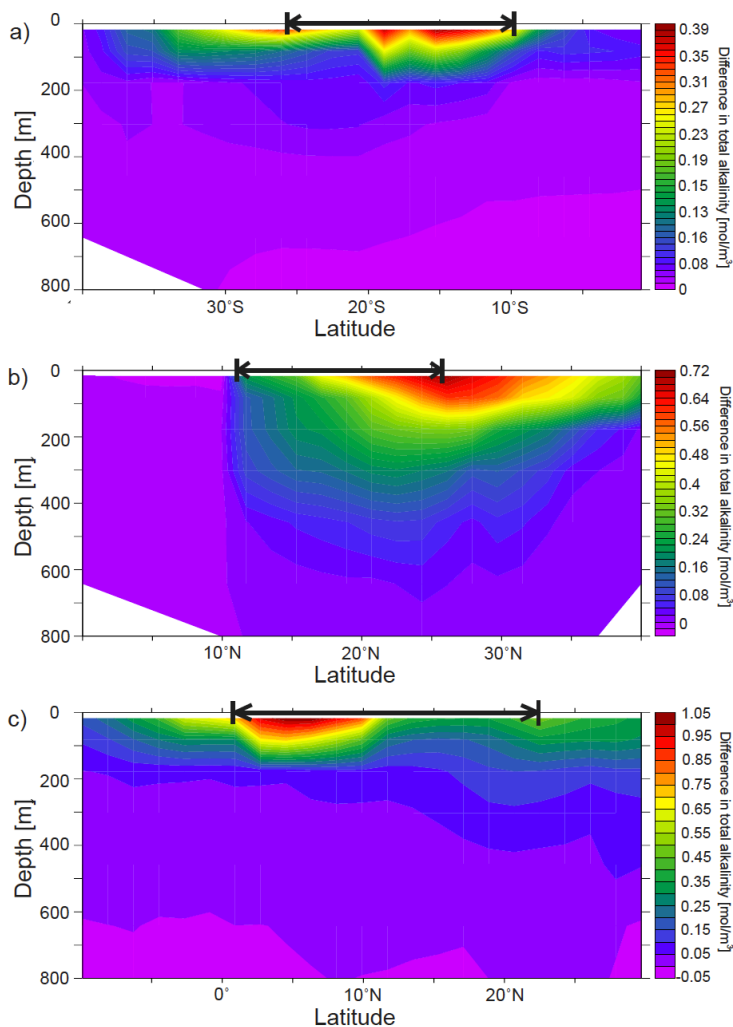
8

9   **Figure S8.** Annual meridional oceanic total alkalinity differences between the optimal AOA

10   runs and the control run in the year 2099. Regions where AOA are implemented: a) Great

11   Barrier Reef, b) Caribbean Sea, and c) South China Sea, are marked within the arrows on the
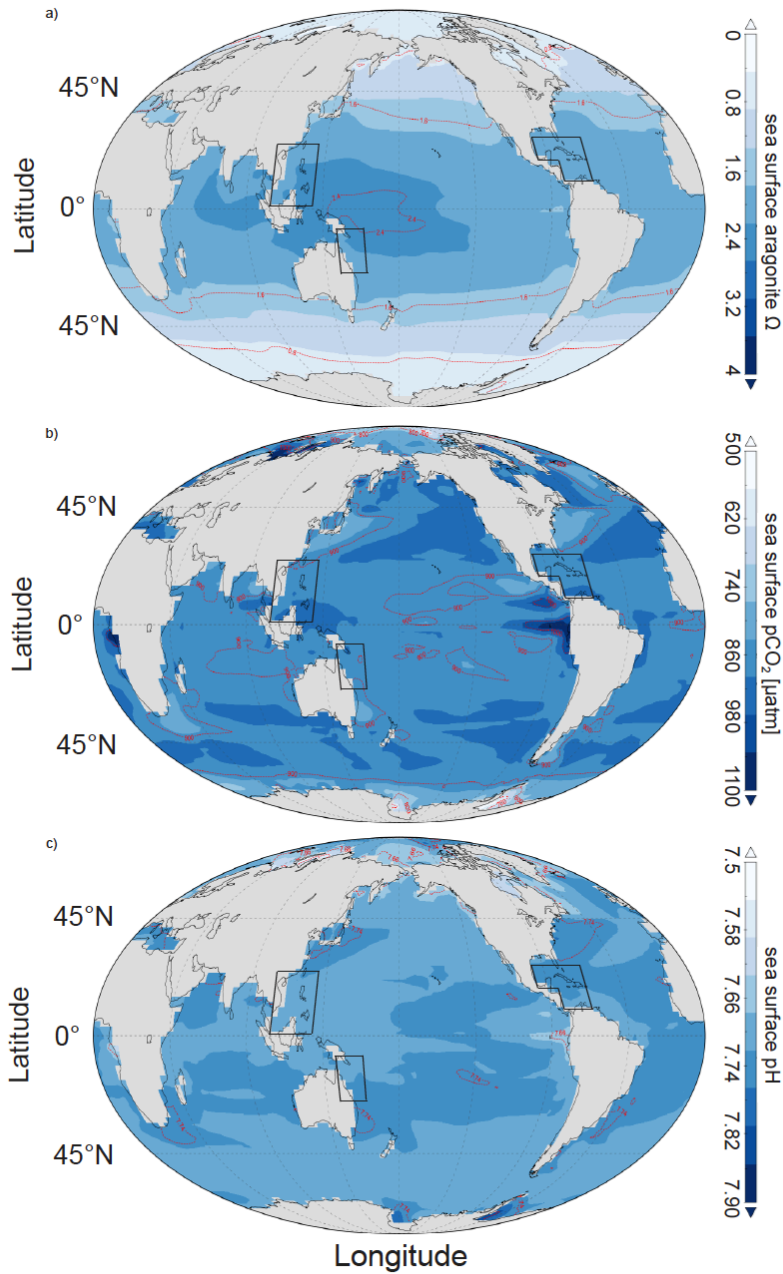
12   top of each subplot.

13

1

2
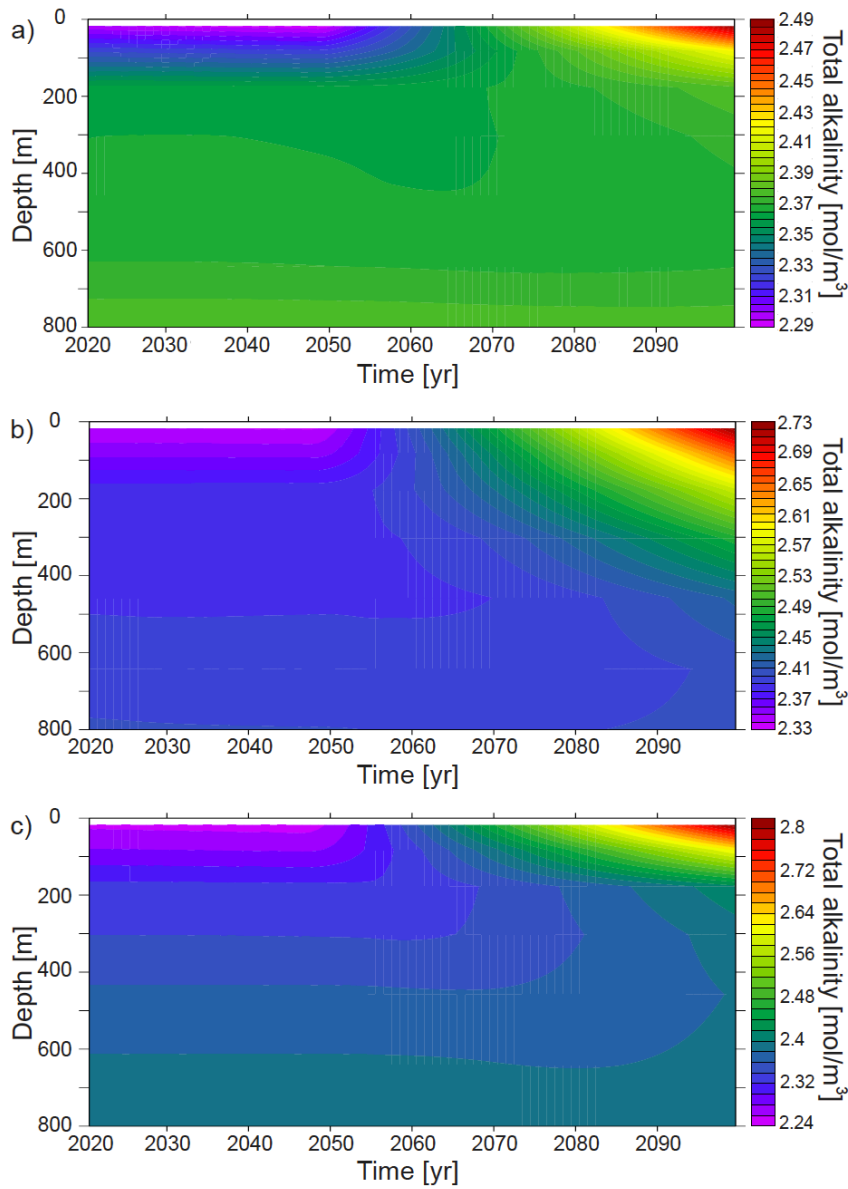
Figure S9 Simulated total alkalinity changes in regional average for AOA implemented

regions: a) Great Barrier Reef, b) Caribbean Sea, and c) South China Sea, from year 2020 to

2099 for optimal runs.

6

1

**6.   Global annual surface plots of the aragonite, pCO$_2$ and pH in the control run.**

3

4

Figure S10 Annual global control run distributions of (a) surface aragonite Ω in the year

2099, (b) surface pCO$_2$ in the year 2099, (c) surface pH in the year 2099. Regions where

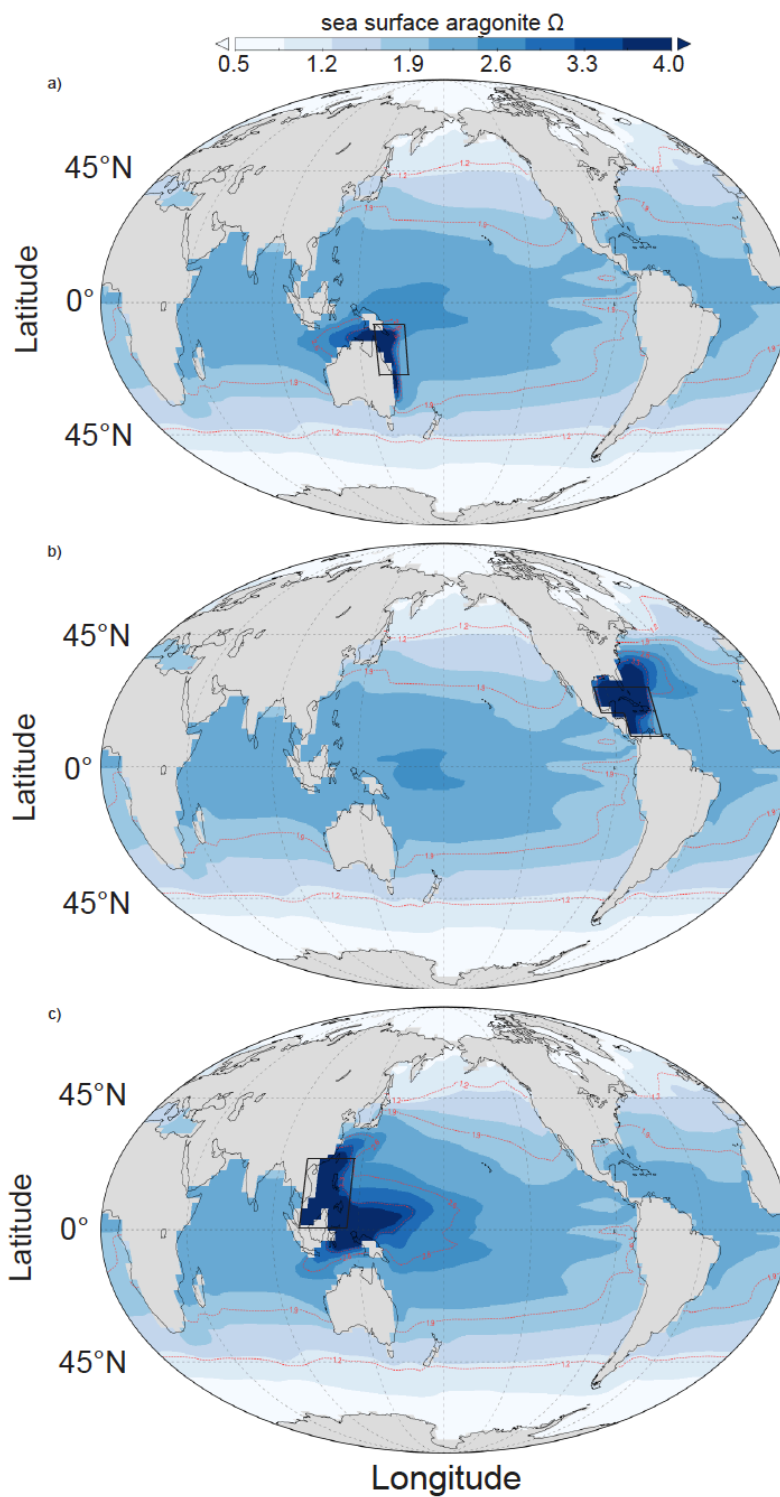AOA is implemented in the experimental runs are marked with boxes.

1   **7.   Global annual surface plots of the pCO_2 and aragonite in the optimal runs.**
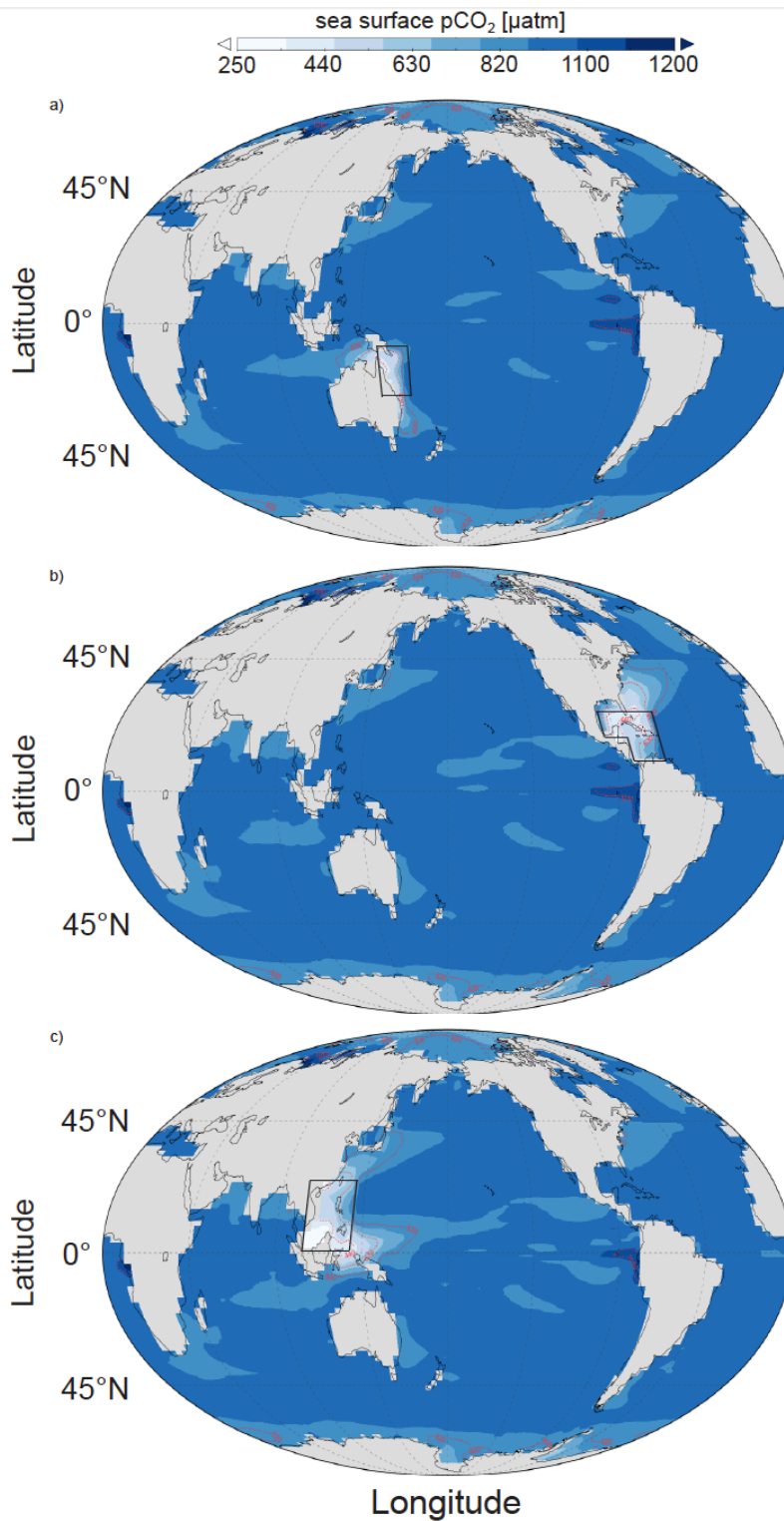
2

3   **Figure S11.** Global annual optimal AOA run distributions of ocean surface pCO_2 in the year

4   2099 in (a) Great Barrier Reef, (b) Caribbean Sea, (c) South China Sea. Regions where AOA

5   is implemented are marked with boxes.

1

Figure S12. Global annual optimal run distributions of the ocean surface aragonite saturation

level in the year 2099 for (a) Great Barrier Reef, (b) Caribbean Sea, (c) South China Sea.

Regions where AOA is implemented are marked with boxes.

8.   A zoomed-in look at the AOA regions

Here we show close-up figures of the AOA regions for the optimal runs in the year 2099 (figure S13). About 36% grid boxes in the GB, 40% in the CS and 58% in the SC have passed the pCO_2=500 regional mean thresholds.
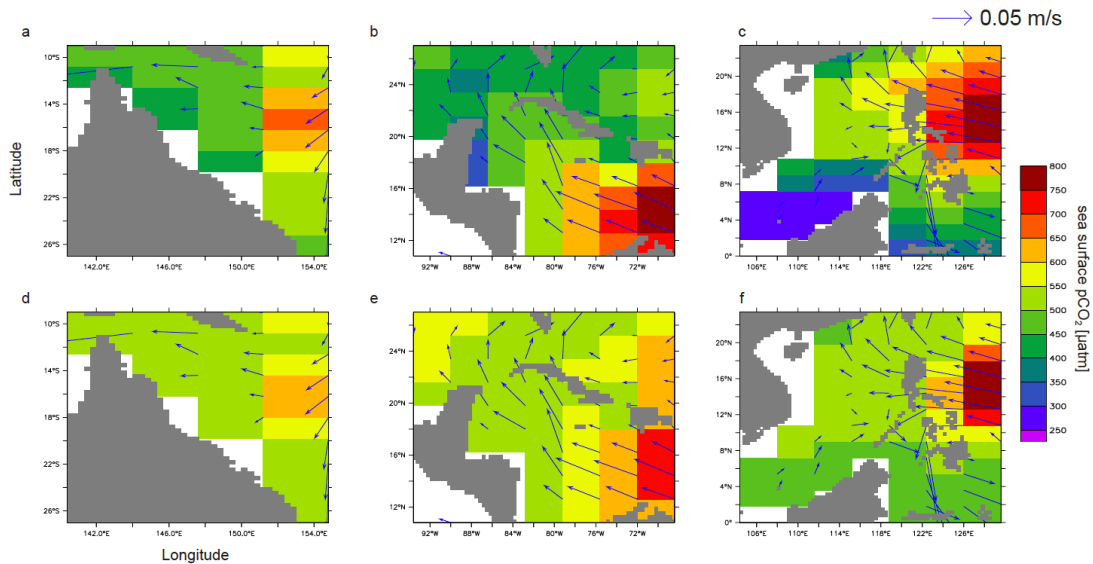
Figure S13. Sea surface annual mean pCO_2 values in year 2099 for AOA regions in our original optimal runs; GB(a), CS(b) and SC(c), with the $pCO_2 = 500$ µatm applied as a regional mean threshold. Another three runs with same configurations as optimal runs, but applying a pCO_2=500 µatm threshold in every grid box are shown for the GB(d), CS(e), and SC(f). These three runs are not discussed in the main text. Sea surface current velocities are shown in arrows.

1 **9.   Global sea surface temperature (SST) and pCO$_2$ anomalies in ENSO year 1988**
2 **(El-Niño year) and 2011 (La-Niña)**

3   Annually averaged SST (*NOAA_OI_SST_V2 data provided by the NOAA/OAR/ESRL*

4 *PSD, Boulder, Colorado, USA, from their Web site at http://www.esrl.noaa.gov/psd/*)

5 (Reynolds *et al* 2002) and surface delta-pCO$_2$ data (Surface Ocean CO$_2$ Atlas, positive values

6 indicate CO$_2$ flux from ocean to atmosphere) (Landschützer *et al* 2014) are used to illustrate

7 the pattern changes of strong El-Niño year (1988) and strong La-Niña year (2011), referenced

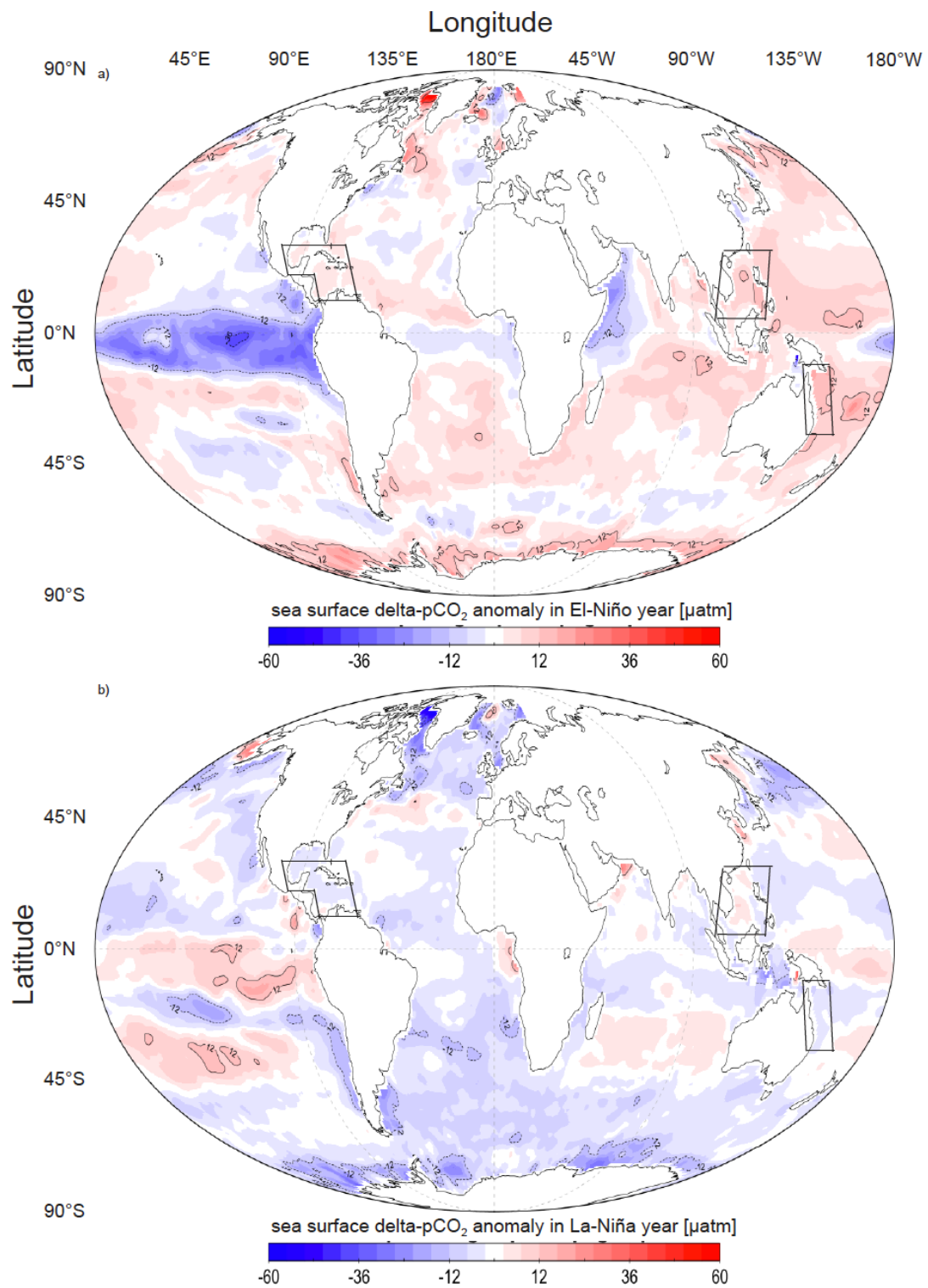8 to climatology data averaged from 1980 to 2011 (figure S14 and S15).

9   We found the regional averaged SST from our studied regions increases around 0.25 °C

10 (Great Barrier Reef region, i.e. GB), 0.15 °C (Carribean Sea, i.e. CS) and 0.34 °C (South

11 China Sea, i.e. SC) in El-Niño year, and 0.14 °C (GB), 0.1 °C (CS) and 0.05 °C (SC) in

12 La-Niña year. The regional averaged surface delta-pCO$_2$ has anomaly of +5µatm (GB), 2µatm

13 (CS) and 9µatm (SC) in El-Niño year, -5µatm (GB), 3µatm (CS), -1µatm (SC) in La-Niña

14 year.

15
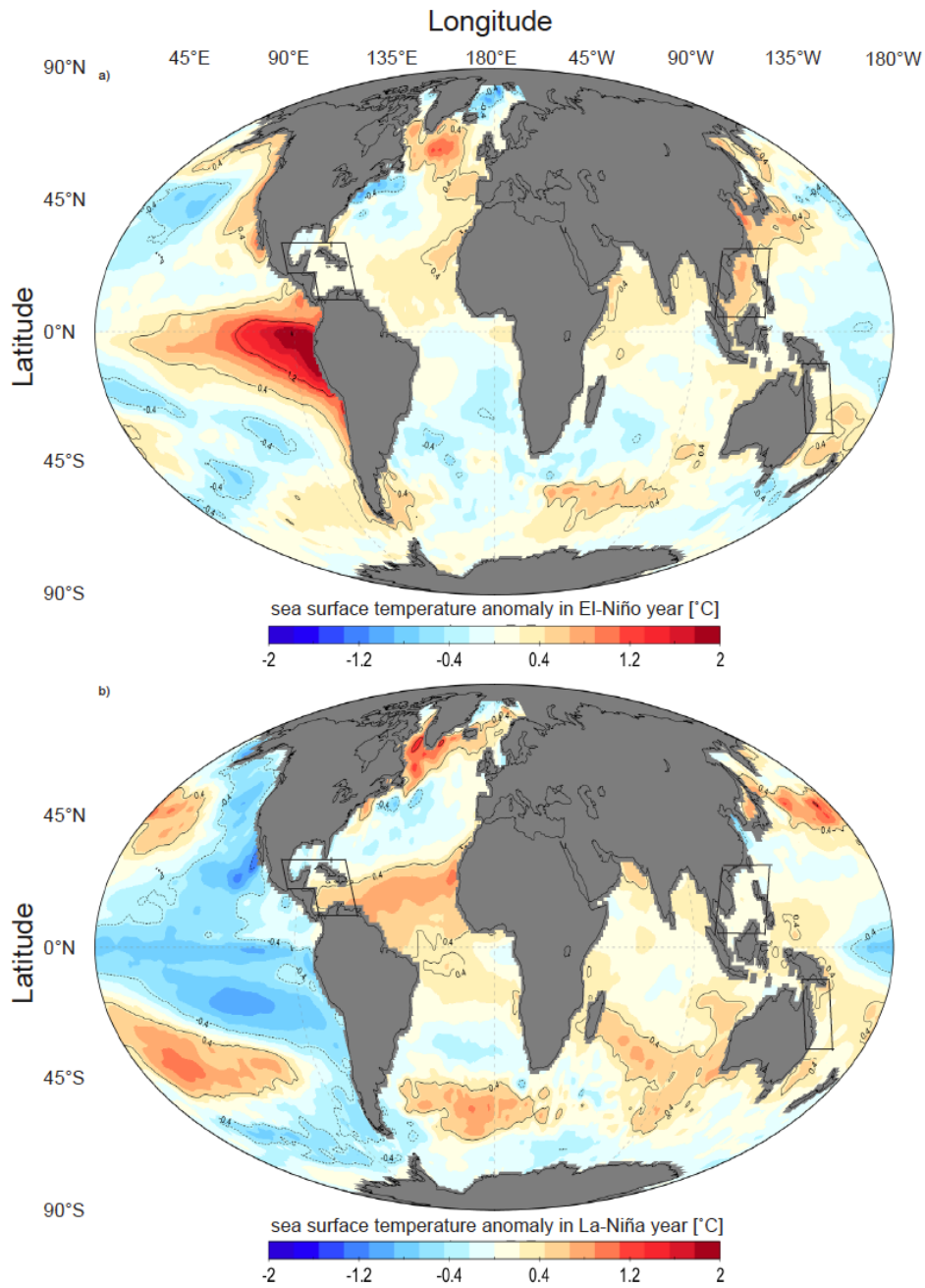
Figure S14. Global annual mean SST anomalies of a) El-Niño year (1998) and b) La-Niña
year (2011) referenced to climatology average from year 1981 to year 2011. Data provided by
the NOAA/OAR/ESRL PSD, Boulder, Colorado, USA, from their Web site at
http://www.esrl.noaa.gov/psd/ (Reynolds *et al* 2002)

Figure S15. Global annual mean delta-pCO$_2$ anomalies of a) El-Niño year (1998) and b) La-Niña year (2011) referenced to climatology average from year 1998 to year 2011 Surface delta-pCO$_2$ data is provided by Surface Ocean CO$_2$ Atlas (positive values indicate CO$_2$ flux from ocean to atmosphere) (Landschützer *et al* 2014)

Supplemental References

 Bakker D C E, et al 2014 An update to the surface ocean CO2 atlas (SOCAT version 2)
     Earth Syst. Sci. Data **6** 69–90

Ilyina T, Six K D, Segschneider J and Maier-reimer E 2013 Global ocean biogeochemistry
     model HAMOCC : Model architecture and performance as component of the MPI-Earth
     system model in different CMIP5 experimental realizations **5** 287–315

Key R M, Kozyr a., Sabine C L, Lee K, Wanninkhof R, Bullister J L, Feely R a., Millero F J,
     Mordy C and Peng T H 2004 A global ocean carbon climatology: Results from Global
     Data Analysis Project (GLODAP) *Global Biogeochem. Cycles* **18** 1–23

Landschützer P, Gruber N, Bakker D C E and Schuster U 2014 Global Biogeochemical
     Cycles 927–49

Locarnini R A, Mishonov A V., Antonov J I, Boyer T P, Garcia H E, Baranova O K, Zweng
     M M, Paver C R, Reagan J R, Johnson D R, Hamilton M and Seidov D 2013 *NOAA
     Atlas NESDIS 62 WORLD OCEAN ATLAS 2013 Volume 1 : Temperature* vol 1 Online:

Pilson M E Q 2013 Major constituents of seawater *An introduction to the chemistry of the sea*
     (Cambridge university press) p 67

Reynolds R W, Rayner N A, Smith T M, Stokes D C and Wang W 2002 An improved in situ
     and satellite SST analysis for climate *J. Clim.* **15** 1609–25

Wang C, Zhang L, Lee S-K, Wu L and Mechoso C R 2014 A global perspective on CMIP5
     climate model biases *Nat. Clim. Chang.* **4** 201–5

Wolf-Gladrow D A, Zeebe R E, Klaas C, Körtzinger A and Dickson A G 2007 Total
     alkalinity: The explicit conservative expression and its application to biogeochemical
     processes *Mar. Chem.* **106** 287–300

Lewis E and Wallace D W R 1998 Program developed for CO2 system calculations, Carbon
     Dioxide Information Analysis Center, Report ORNL/CDIAC-105 (Oak Ridge National
     Laboratory, Oak Ridge, TN, USA)

van Heuven S, Pierrot D, Lewis E and Wallace D W R 2009 MATLAB Program Developed
     for CO2 System Calculations, ORNL/CDIAC-105b, Carbon Dioxide Information
     Analysis Center (Oak Ridge National Laboratory, Oak Ridge, TN, USA)